TRAVELING-WAVE PHOTOMIXERS BASED ON NONCOLLINEAR OPTICAL/TERAHERTZ PHASE-MATCHING

Shuji Matsuura and Geoffrey A. Blake
Division of Geological and Planetary Sciences, California Institute of Technology, Pasadena, CA 91125

Rolf A. Wyss and J. C. Pearson
Jet Propulsion Laboratory, California Institute of Technology, Pasadena, CA 91109

Christoph Kadow, Andrew W. Jackson and Arthur C. Gossard
Materials Department, University of California, Santa Barbara, CA 93106

Abstract

Traveling-wave THz photomixers based on angle-tuned optical/THz phase-matching are experimentally demonstrated. A dc-biased coplanar stripline terminated by a planar antenna is fabricated on low-temperature-grown GaAs. A distributed area between the striplines is illuminated by two noncollinear laser beams which generate interference fringes accompanied by THz waves. The velocity of the optical fringe is matched to the THz-wave velocity in the stripline by tuning the incident angle of the laser beams. The device can handle the laser power over 300 mW and provides the THz output of ~0.1 μW with the 3-dB bandwidth of 2 THz. The experimental results show that traveling-wave photomixers have the potential to surpass conventional small area designs.

1. Introduction

The difference frequency generation of THz waves by optical-heterodyne (photo) mixing in low-temperature-grown (LTG) GaAs has been investigated as a highly tunable, compact, solid-state THz source for high-resolution molecular spectroscopy and as a local oscillator for heterodyne receivers in remote-sensing applications.[1-5] The spectral purity and frequency stability of the THz output is basically determined by the pump laser source, and sufficiently high performance has now been achieved.[6,7] However, the THz output power has been limited to less than 1 μW above 1 THz, which is insufficient for many applications.

According to a photomixer theory,[1] the photomixer output power is proportional to the square of the photocurrent, which is proportional to both the pump laser power and the photoconductance. On the other hand, for conventional photomixers, the bandwidth is limited by the carrier lifetime and the electrode capacitance.[1] Since both the photoconductance and the capacitance are inversely proportional to the electrode gap width, photomixers have been designed to have small active areas ($\leq 10^2$ μm^2). However, such designs have limited power handling capabilities,[5] thus restricting the THz output power. The thermal damage threshold of typical LTG-GaAs film is <2 mW/μm^2, and the maximum laser power has been limited to ≤100 mW.

In order to overcome this difficulty, we propose a large area traveling-wave photomixer design. The device consists of a dc-biased coplanar stripline terminated by an antenna

fabricated on the LTG-GaAs. The ~10^3 μm^2 area in the stripline gap is illuminated by noncollinear two laser beams. The photocarrier density traveling-waves induced by the optical interference fringes are generated in the stripline and accompanied by the THz waves. The THz waves are transmitted to the antenna through the stripline. Owing to large active area, the laser power handling capability of the order of 1 W is expected. The traveling-wave photomixer not only has high power handling capability, but its bandwidth is also not limited by the electrode capacitance because of the nature of stripline. As high power laser sources are improved, the traveling-wave photomixer can provide good THz output with wide bandwidths, and should ultimately be superior to conventional small area photomixers.

For traveling-wave photomixers, the velocity (phase) matching between the optical interference fringes and the THz waves is essential for efficient THz wave generation. Under the phase-matching condition, the THz waves from the distributed active area are superposed in phase in the stripline. Several authors have achieved phase-matching between optical waves and microwaves in traveling-wave optical waveguide photodetectors, which slow down the microwave velocity with periodic capacitance loading of the microwave transmission line.[8,9] Such a phase-matched waveguide photomixer requires careful design and fabrication because of its fixed structure, and these devices have not yet been extended to the THz range. We propose the noncollinear optical/THz phase-matching scheme for the free space traveling-wave photomixer, which does not require such complicated waveguide structure. In this method, the velocity of the optical wave is tuned by changing the incident angle of the two laser beams.

In this paper, the phase-matching scheme is briefly described and experimentally demonstrated. The device properties and future direction for the output power improvement are discussed.

2. Optical/THz phase-matching

As described above, the phase-matching is achieved by tuning the incident angle of the two laser beams. In order to formulate the phase-matching condition, we consider a simple picture as shown in Fig. 1. When the photomixer surface is illuminated by two plane waves of

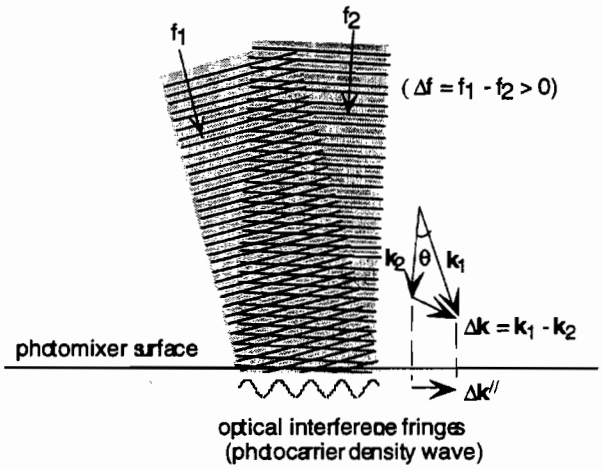

Fig. 1: Optical/THz phase-matching scheme.

frequency f_1 and f_2, and the wave vector of $\boldsymbol{k}_1$ and $\boldsymbol{k}_2$, respectively, the propagation constant of the interference fringe oscillating at the difference frequency, $\Delta f = f_1 - f_2$, is given by the parallel (//) component of the difference of the two wave vectors, $\Delta \boldsymbol{k} = \boldsymbol{k}_1 - \boldsymbol{k}_2$. Since absorption occurs in a thin surface layer (penetration depth ~1 μm), the photocarriers have the same spatial distribution as the optical interference fringes. The velocity of the interference fringes along the surface is given by

$$v_{op} = 2\pi \frac{\Delta f}{\Delta k^{//}} \ . \tag{1}$$

It is clear that the velocity can be tuned by changing the incident angles of the optical beams. In a simple case that $\boldsymbol{k}_2$ is perpendicular to the photomixer surface, Eq. 1 can be written as

$$v_{op} = \frac{c}{\sin\theta}\left(1 - \frac{f_2}{f_1}\right) , \tag{1'}$$

where c is the speed of light in the free space and θ is the incident angle of the f_1 laser beam. If it is assumed that the stripline has no dispersion, the velocity of the THz wave is approximated by

$$v_{THz} \approx \frac{c}{\sqrt{(1+\varepsilon_r)/2}} , \tag{2}$$

where ε_r is dielectric constant of the substrate material (ε_r = 12.8 for GaAs). The phase-matching condition is $v_{op} = v_{THz}$.

3. Photomixer

The photomixer used in the present experiment is a 1-μm thick LTG-GaAs film grown on semi-insulating GaAs substrates by molecular beam epitaxy (MBE) at a temperature of 225° C. Diffuse Reflectance Spectroscopy (DRS) was used to maintain the substrate temperature within 5° C of the setpoint through the growth. The material was annealed ex situ by rapid thermal annealing (RTA) for 30 s at 600° C in a forming gas environment. The photocarrier lifetime of the material measured by time resolved reflectance was 0.28 ps. The device structure is shown in Fig. 2. The Ti/Pt/Au metal electrodes (0.02/0.02/0.2 μm thickness) fabricated on the LTG-GaAs consist of a 2-μm gap and 4-μm wide coplanar stripline. The stripline is terminated by a 47-μm long and 5-μm wide dipole antenna or a log-periodic antenna. The other side of the stripline is terminated by wire bonding pads for the dc bias,

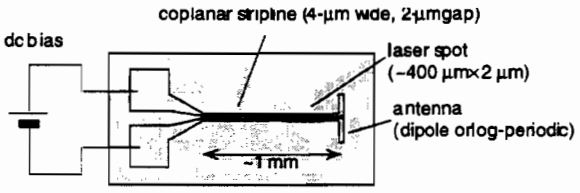

Fig. 2: LTG-GaAs traveling-wave photomixer.

which has tapered shape to reduce the reflection. Most of the THz output power from the antenna goes into the substrate and is emitted to the free space through a hyper-hemispherical high-resistivity silicon lens attached to the back side of the substrate.

4. Experimental setup

The experimental setup for the device characterization is shown in Fig. 3. The optical source is a two-frequency master oscillator power amplifier (MOPA) 850 nm semiconductor laser system. A tapered semiconductor optical amplifier is simultaneously injection-seeded by a tunable external cavity laser (λ_1 = 848-853 nm) and a cavity-locked fixed frequency laser (λ_2 = 854 nm), and provides a maximum two-frequency power of 500 mW.[10] The output from the MOPA is split into two beams by a 2000-groove/mm diffraction grating. The advantage of the split collinear beam over two individual lasers is the nearly identical spatial mode quality of the two colors, which is essential for efficient THz wave generation.

For a grating incidence angle of $\alpha = 50^\circ$, the 1st order diffraction angle and its dispersion is $\beta = 70^\circ$ and $d\beta/df = 0.8^\circ$ THz^{-1}, respectively. At this configuration the diffraction efficiency is about 80%. The diffracted beams are reflected by two plane mirrors and focused onto the photomixer by a 6-mm-focal-length cylindrical lens. The ~2-mm diameter circular MOPA beam is compressed to a ~0.4 mm × 2 mm elliptical beam by the grating. The maximum available laser power after the grating is ~300 mW.

In the present implementation, the incident angle of the fixed frequency laser beam is set to zero (perpendicular to the photomixer surface). For the GaAs substrate, the phase-matching condition is fulfilled when the angle separation between the two laser beams, θ, is approximately half the dispersion angle of the two beams, or $\theta \cong 0.5\Delta\beta$. The angle and position of the mirror M_1 is adjusted to overlap the two laser beams at the photomixer surface. The THz output power was measured with a silicon composite bolometer placed ~3 cm from

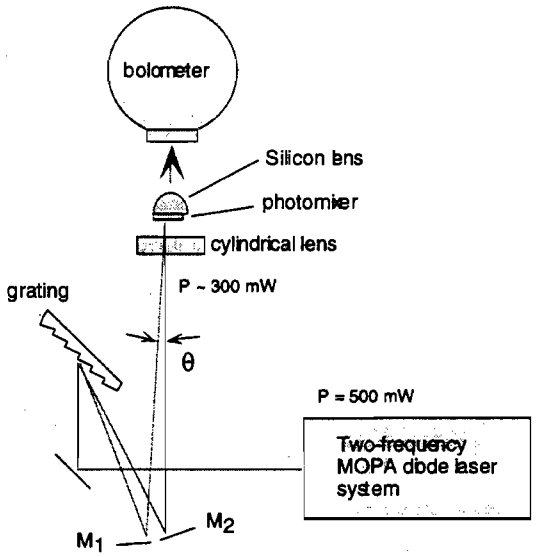

Fig. 3: Experimental setup.

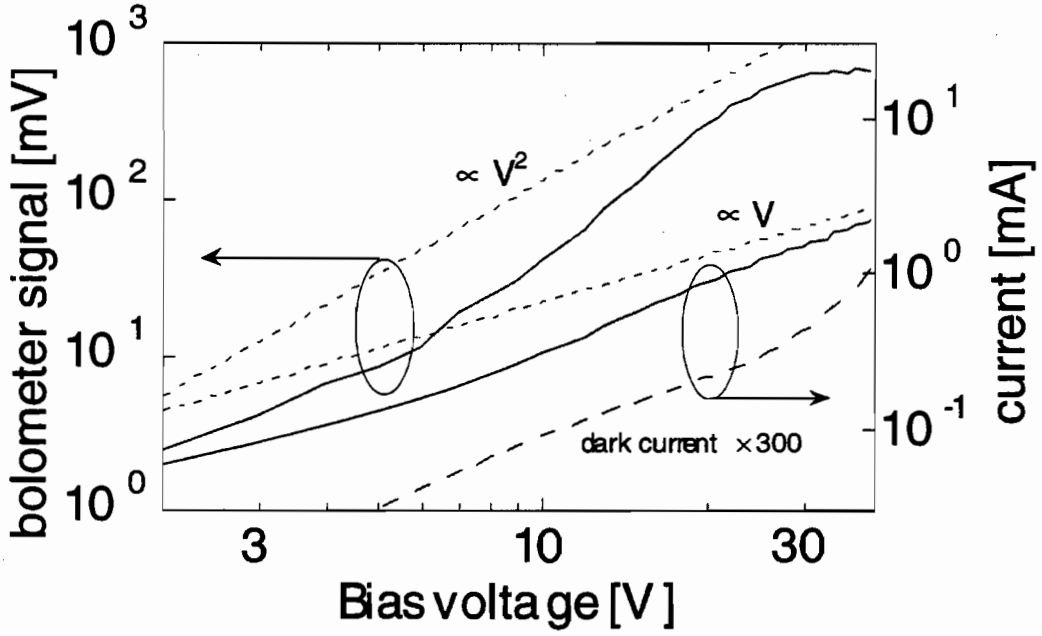

Fig. 4: The bias voltage dependence of the dc-photocurrent, dark current, and the THz output at f = 1 THz.

the photomixer by chopping the laser beams at 100 Hz. Thermal emission caused by the laser and electrical power was estimated from the bolometer signal when one laser beam was blocked.

5. Results and discussions

5-1. *Bias dependence*

Shown in Fig. 4 is the bias voltage dependence of the dc-photocurrent of the log-periodic antenna photomixer and the THz output measured at 1 THz under the phase-matching condition. The pump laser power is 280 mW at the photomixer surface. The dc-photocurrent shows a super-linear dependence, whereas linear (ohmic) dependence is expected, for the bias voltage greater than 5 V which corresponds to $E > 2.5\times10^4$ V/cm . The quadratic or super-linear dependence of the photocurrent has been seen in LTG-GaAs photomixers with sub-μm electrodes at high bias fields ($E > 10^5$ V/cm), where the space-charge-limited currents take place.[2,5] The data shows a super-linear dependence even at low bias voltage, which might arise here, because the photon or photocarrier density in the active area is ~5 times lower than that for small area photomixers. The space-charge-limited current is basically slow phenomenon and increases the dc current greatly but does not contribute to the ac current, which generates the THz wave. However, the THz output shows a super-quadratic dependence and it obeys the photocurrent square law[1] below 20 V, as seen in Fig. 4. The super-linear dependence of the photocurrent might be caused by the other effects such as

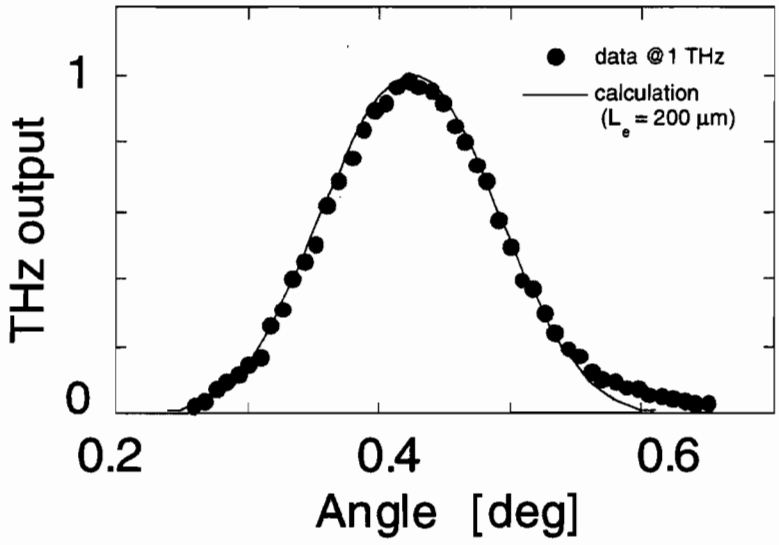

Fig. 5: The phase mismatch curve at f = 1 THz.

potential barrier at the metal contact. The THz output shows the saturation above 20 V, and the 'knee' voltage agrees with the breakdown voltage seen in the dark current curve. However, the dark current could not smooth out the photocarrier density waves directly, because it is the order of 10^{-3} of the photocurrent. Such saturation effect has been seen for small area photomixers and practically eliminated or reduced by increasing the laser power.[11] In order to clarify the saturation mechanism and improve the output power, more detailed theoretical consideration and further measurements under much higher photon density condition are required.

5-2. *Phase-matching*

For traveling-wave photomixers, the THz output power decreases with increasing the phase mismatch. Fig. 5 presents the THz output dependence on the incident angle of the f_1 laser, measured at 1 THz for the dipole device. The data show a maximum at $\theta = 0.42°$, which is close to that expected from Eq. 1 and 2. If it is assumed that the laser power density is uniform over the whole active area of the photomixer, the ac photocurrent integrated over the active area is expressed as a *sinc* function, and the THz output power is then given by

$$P_{THz} = A\left(\frac{\sin^2(\Delta kL/2)}{(\Delta kL/2)^2}\right)^2 , \tag{3a}$$

where Δk is the phase mismatch,

$$\Delta k = 2\pi f\left(\frac{1}{v_{THz}} - \frac{1}{v_{op}}\right) , \tag{3b}$$

A is a constant, and L is the length of active area of the photomixer. The calculated profile for L = 200 μm, shown by the solid curve in Fig. 5, shows good agreement with the data. The

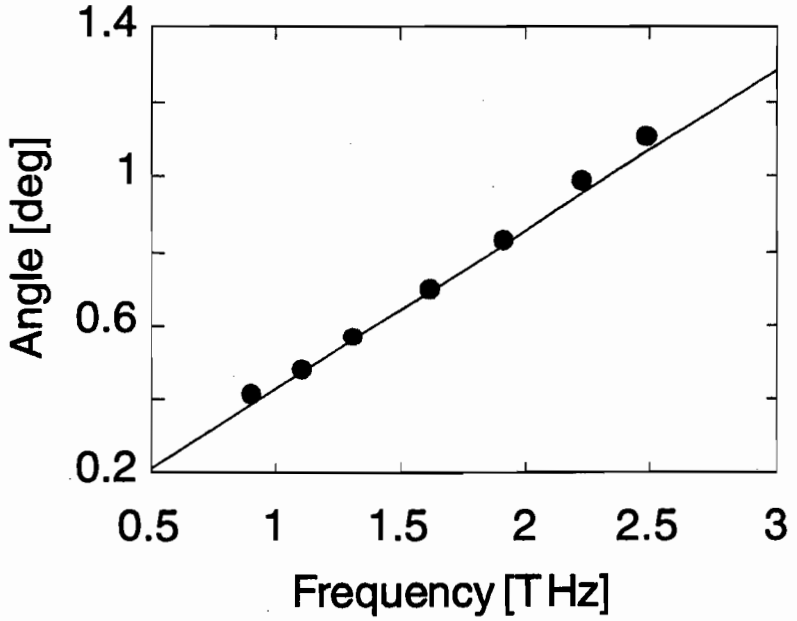

Fig. 6: The phase-matching angle vs the THz-wave frequency. The solid line is calculated from Eq. 1 and 2.

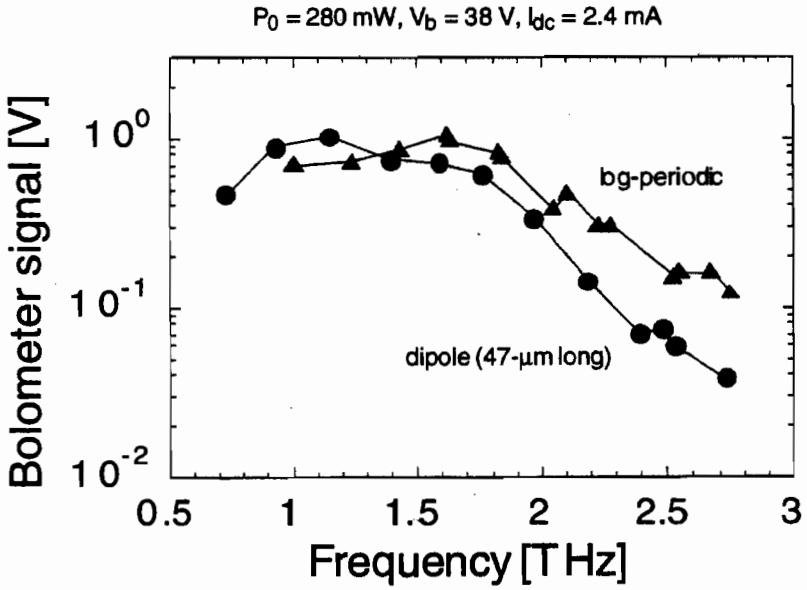

Fig. 7: The THz output spectrum of the dipole antenna device (circles) and the log-periodic antenna device (triangles).

effective active area would be smaller than the estimated laser spot size of ~400 μm, because the laser beam has a gaussian distribution rather than uniform distribution.

According to Eq. 1 for small θ, the angle mismatch curve, shown in Fig. 5, is independent on the THz-wave frequency. In fact, the measured mismatch curve was almost frequency independent. In Fig. 6 the phase-matching angle is plotted against the frequency. The data show good agreement with the tuning coefficient of 0.42° THz^{-1} predicted from Eq. 1 and 2, indicated by the solid line. Small scatter of the data from the predicted line might be due to the dispersion of the stripline. These results shown in Fig. 5 and 6 demonstrate that the present device works as a (phase-matched) distributed device.

5-3. *THz output spectrum*

The THz output spectra for both the dipole device and the log-periodic device are shown in Fig. 7. As noted above, the bandwidth of the ideal traveling-wave photomixer should be determined mainly by the LTG-GaAs carrier lifetime, which rolls-off as 6 dB/Oct. However, the data show a 3-dB bandwidth of 1.8 THz for the dipole and 2 THz for the log-periodic, which exceed the carrier-lifetime-limited bandwidth of 600 GHz, and a roll-off of ≥10 dB/Oct, similar to that of small area photomixers.[1] The spectral difference between the two devices is mainly due to the antenna impedance difference. The impedance of the log-periodic

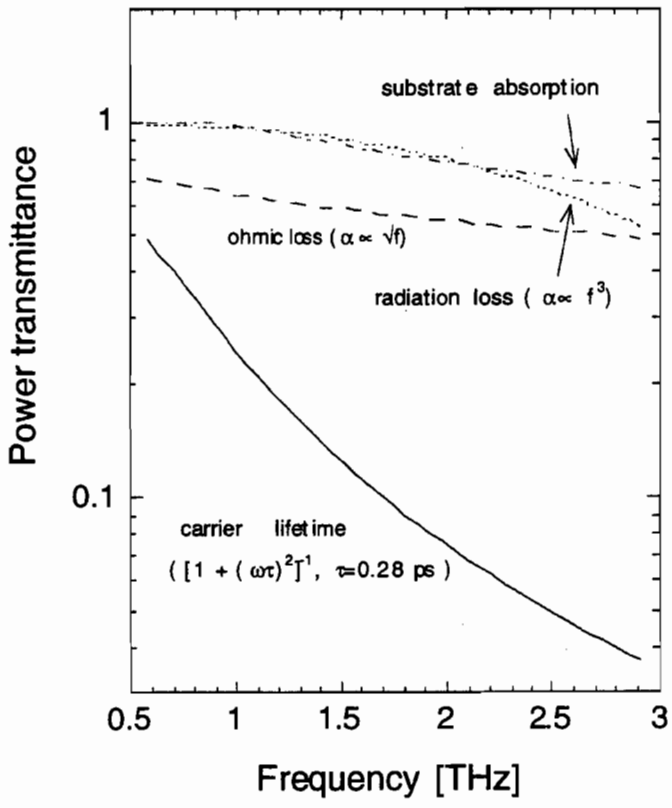

Fig. 8: The calculation of various losses; the carrier lifetime roll-off, conductor (ohmic) loss of the stripline metal, the radiation loss, and the substrate loss (the dielectric loss and the substrate transmittance).

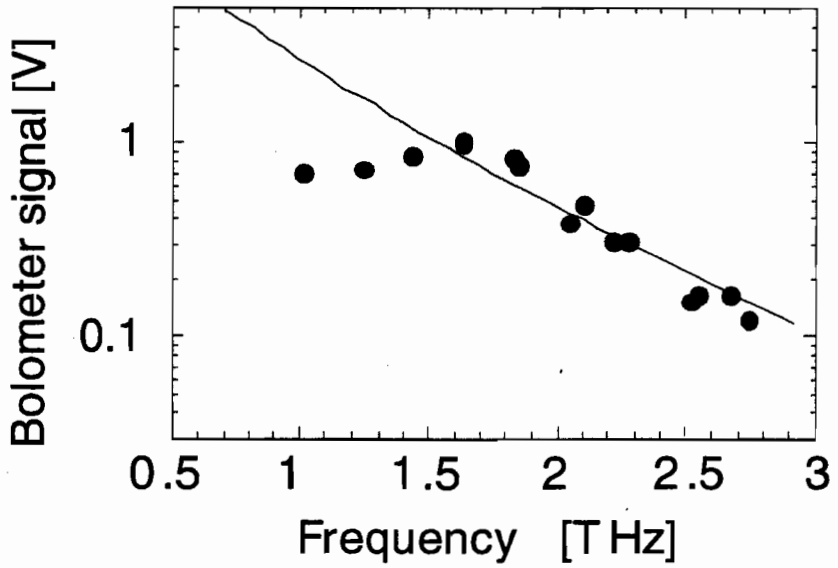

Fig. 9: The comparison between the data for the log-periodic device (circles) and the calculation (solid curve).

of 72 Ω is well-matched to the stripline impedance of 76Ω, while the dipole impedance is frequency dependent and matched to the stripline impedance only at restricted frequencies.

The additional roll-off can be interpreted as that arising from the conductor (ohmic) loss and radiation loss in the transmission line, and the substrate absorption. The conductor loss[12] calculated from the skin-effect resistance is $10\sqrt{f}$ dB/mm, where f is the frequency in THz. The radiation loss[13] is calculated to be $0.6f^3$ dB/mm. The substrate absorption measured with the FT-IR spectrometer is less than 2 dB/mm at ≤3 THz. Fig. 8 presents the THz power transmittance for the 400-μm long stripline calculated from these losses, assuming the THz-waves are uniformly generated in the active area. The total loss other than the carrier lifetime roll-off is less than 8 dB at ≤3 THz.

Fig. 9 presents the calculated spectrum for the log-periodic device, taking into account the carrier lifetime and the losses described above. The calculation shows rough agreement with the data, but the measured bandwidth is much wider than the calculation, due to the presence of a flat region at 1-2 THz. In order to clarify the details of the device property, further measurements for the devices with various electrode structures and detailed analysis are required. The bolometer signal of 1 V in Fig. 9 corresponds to ~0.1 μW, while the output power is predicted to be >4 μW at 1.5 THz for a dc-photocurrent of 2.4 mA. At present, the cause of this large discrepancy is not clear. It might be due to a shallow depth of the optical interference fringes and a effect which causes the output saturation at high bias end as described in 5-1.

6. Future direction

There are several practical ways to increase the THz output power. One is the increase of the laser power. Since the laser power density per unit area is presently ~1/5 of the thermal

damage threshold, the increase of the laser power reflects directly the THz output power. The increase of the laser power density may also contribute to the output power improvement, because the output saturation effect could be reduced by increasing the laser power density, as described above. This can be done by shortening the active area length (laser spot size), and it contribute to reduce the stripline loss, too. Another way is increasing the photoconductivity by narrowing the stripline gap. If the 1-μm gap device is used, the output power increases by a factor of 4, though the ohmic loss would increase and cancel the power gain a little. In addition, the radiation loss can be reduced by narrowing the total stripline width, and the substrate absorption can be eliminated by employing a silicon substrate. The silicon based photomixer offers additional benefit of high power handling capability.[5] By combining these power gain factors, one order of magnitude output power improvement would be achieved.

Acknowledgment

The authors would like to thank T. E. Turner in the Microelectronics Device Laboratory at JPL for device fabrication. This research was sponsored by the Jet Propulsion Laboratory, California Institute of Technology, and the National Aeronautics and Space Administration. The work performed at UCSB was supported by the Center for Nonstoichiometric III-V Semiconductors.

References

[1] E. R. Brown, F. W. Smith, and K. A. McIntosh, *J. Appl. Phys.*, **73**, 1480 (1993).

[2] E. R. Brown, K. A. McIntosh, F. W. Smith, K. B. Nichols, M. J. Manfra, C. L. Dennis, and J. P. Mattia, *Appl. Phys. Lett.*, **64**, 3311 (1994).

[3] K. A. McIntosh, E. R. Brown, K. B. Nichols, O. B. McMahon, W. F. DiNatale, and T. M. Lyszczarz, *Appl. Phys. Lett.*, **67**, 3844 (1995).

[4] S. Matsuura, M. Tani, and K. Sakai, *Appl. Phys. Lett.*, **70**, 559, (1997).

[5] S. Verghese, K.A. McIntosh, and E.R. Brown, *IEEE Trans. Microwave Theory and Tech.*, **45**, 1301 (1997).

[6] P. Chen, G. A. Blake, M. C. Gaidis, E. R. Brown, K. A. McIntosh, S. Y. Chou, M. I. Nathan, and F. Williamson, *Appl. Phys. Lett.* **71**, 1601 (1997).

[7] S. Matsuura, P. Chen, G. A. Blake, J. C. Pearson, and H. M. Pickett, , *IEEE Trans. Microwave Theory and Tech.*, (1999), in press.

[8] L. Y. Lin, M. C. Wu, T. Itoh, T. A. Vang, R. E. Muller, D. L. Sivco, and A. Y. Cho, *IEEE Phton. Technol. Lett.*, **8**, 1376 (1996).

[9] Y. -J. Chiu, S. B. Fleischer, and J. E. Bowers, *IEEE Phton. Technol. Lett.*, **10**, 1021 (1998).

[10] S. Matsuura, P. Chen, G. A. Blake, J. C. Pearson, and H. M. Pickett, Int. *J. of Infrared and Millimeter Waves*, **19**, 849 (1998).

[11] S. Verghese, private communication.

[12] K. C. Gupta, R. Garg, and R. Chadha, *Computer-aided Design of Microwave Circuits*, (Artech House, Norwood, MA, 1981), p. 72.

[13] D. B. Rutledge, D. P. Neikirk, and D. P. Kasilingam, in *Infrared and Millimeter Waves*, edited by K. J. Button (Academic Press, New York 1983), Vol. 10, p. 1.